Microchimica Acta (2019) 186: 332
https://doi.org/10.1007/s00604-019-3439-0

ORIGINAL PAPER

Perylene diimide-functionalized CeO_2 nanocomposite as a peroxidase mimic for colorimetric determination of hydrogen peroxide and glutathione

Jiajia Lian[1,2] · Pei Liu[1,2] · Chunqiao Jin[1,2] · Zhiqiang Shi[3] · Xiliang Luo[4,5] · Qingyun Liu[1,2]

Received: 3 January 2019 / Accepted: 12 April 2019 / Published online: 6 May 2019

Abstract

A novel perylene diimide (PDI) functionalized CeO_2 nanocomposite (NC) was successfully fabricated via one-pot hydrothermal method. Compared with pure CeO_2 nanoparticles (CeO_2 NPs), the NC catalyst presents more Ce^{3+} and active oxygen species and exhibits a higher peroxidase mimicking activity towards the oxidation 3,3′,5,5′-tetramethylbenzidine by H_2O_2 to form a blue product with an absorption maximum at 652 nm. The composite catalyst shows high sensitivity and selectivity toward H_2O_2 determination in the range of 20 to 80 μM with a limit of detection (LOD) of 2.59 μM. Based on the colorimetric method, a sensitive method for detecting the reduced glutathione (GSH) was also established over arrange of 1~4 μM with a LOD of 0.92 μM. Electron spin resonance (ESR) experiments suggest that the active radicals during the catalytic processes are •OH and $•O_2^-$. A possible synergistic catalytic mechanism is discussed.

Keywords Perylene diimide · Ceria · One-pot hydrothermal · Peroxidase · Mechanism

Introduction

Due to the high cost and low stability of natural enzymes for detecting H_2O_2 in harsh environments, many artificial peroxide mimetic enzymes have been exploited. It has been proved that various materials possess peroxidase-like activities, such as noble metals [1–3], metal oxides [4, 5], metal sulfide [6–8] and metal-organic hybrids [9–11]. Nano-ceria (CeO_2) has been attracted significant interest due to the exposed Ce^{3+} ions are surface sites for catalysis and O-vacancies favor to the migration and transformation of active species [12]. For example, the superior catalytic performance of 6%Fe^{3+}-doped CeO_2 (6Fe/CeO_2) NRs are attributed to the abundant surface defects, high surface area and pore volume [13]. The Fe_3O_4@CeO_2 yolk-shell nanocomposite can produce more hydroxyl radicals (•OH) in the presence of H_2O_2 [14]. The presence of CeO_2 uniformly covered on the oxidized single-walled carbon nano-horns (ox-SWCNHs) guarantees an efficient electronic communication [15].

Jiajia Lian and Pei Liu contributed equally to this paper and share the first authorship.

Electronic supplementary material The online version of this article (https://doi.org/10.1007/s00604-019-3439-0) contains supplementary material, which is available to authorized users.

✉ Qingyun Liu
qyliu@sdust.edu.cn

[1] College of Chemical and Environmental Engineering, Shandong University of Science and Technology, Qingdao 266590, China

[2] State Key Laboratory of Mining Disaster Prevention and Control Co-founded by Shandong Province and the Ministry of Science and Technology, Shandong University of Science and Technology, Qingdao 266590, China

[3] School of Chemistry, Chemical Engineering and Materials, Shandong Normal University, Jinan 250013, People's Republic of China

[4] Shandong Key Laboratory of Biochemical Analysis, Qingdao University of Science and Technology, Qingdao 266042, People's Republic of China

[5] College of Chemistry and Molecular Engineering, Qingdao University of Science and Technology, Qingdao 266042, People's Republic of China

The formation of more Ce^{3+} ions associated with the oxygen vacancies as well as a strong synergistic interaction between CeO_2 and Co_3O_4 may be responsible for the enhanced peroxidase-like activity [16]. Although the catalytic activity of such materials is obviously enhanced, it still remains several obvious shortcomings. For instance, the metal-based materials give rise to the high cost of noble metals or toxicity of heavy metals [17]. And the dispersion/stability is still a problem, because the loading of high density metals/metal oxides makes the hybrids easy to agglomerate. Therefore, to overcome these drawbacks, a novel material should be built to decorate the CeO_2 NPs.

A new type of photosensitive dyes, perylene diimide (PDI), have been extensively studied and applied in photocatalytic and organic solar cells, due to their excellent adsorption, chemical and thermal stabilities, strong electron-withdrawing ability and high electron mobility [18, 19]. The charge and hole transfer rates of PDI and its derivatives are higher than that of the typical electron and hole transport materials [20]. The PDI/Copper phthalocyanine (CuTcPc) heterostructure facilitates the electron transfer from PDI to CuTcPc, thus resulting in the effective separation of photogenerated electron-hole pairs [21]. And the formation of the PDI-metal complexes with Pt(II) and Pd(II) lead to strong intramolecular charge transfer [22]. Therefore, the combination of PDI and CeO_2 NPs can not only retain the excellent electron transfer properties of PDI but the strong redox behavior and surface defects of nanoceria. And to the best of our knowledge, there is no report on the peroxidase-like activity of PDI decorated CeO_2 NPs.

In this paper, the uniform NC was fabricated via a one-pot hydrothermal route, and performed on the colorimetric determination of H_2O_2 and GSH. The NC exhibits high catalytic activity and excellent stability. The low limits of detection and high selectivity made NC a promising assay for H_2O_2 and GSH detection. The synergistic catalytic mechanism that NC catalyzed H_2O_2 to oxidize TMB was also studied here.

Experimental

Materials

$Ce(NO_3)_3$•$6H_2O$ and H_2O_2 (30%, *w*/w) were purchased from Sinopharm Chemical Reagent Co. Ltd. (Shanghai, http://www.sinoreagent.com). Perylene diimide (PDI) with four carboxyl was synthesized according to the previous report [23]. TMB was purchased from Macklin (http://www.macklin.cn/). Horseradish peroxidase (HRP), D-serine (Ser), Urio acid (UA), L-Arginine (Arg), D-Histidine (His), D-Leucine (Leu), DL-ISOLeucine (ISO), DL-Tryptophan (Try) and GSH were obtained from Aldrich (www.sigmaaldrich.com). The medical GSH pills (93.34 wt.%) were purchased from Shandong Luye Pharmaceutical Co., Ltd. (http://www.luye.cn/lvye/). All reagents were of analytical reagent grade and used without further purification. Solutions were prepared with ultrapure water.

Preparation of the nanocomposite (NC)

The NC was prepared by a one-pot hydrothermal method. Briefly, 1.085 g $Ce(NO_3)_3$•$6H_2O$ and 2 mL H_2O_2 (30 wt.%) were added into 40 mL ultrapure water under vigorously stirring at room temperature for 60 min. Then 20 mg PDI powder was well dispersed into 20 mL ultrapure water and slowly dropped into the mixed system above, and vigorously stirred for another 60 min. After that the reaction system was moved into Teflon-lined stainless steel autoclave and heated at 150 °C for 10 h. After cooling to room temperature, the sample was centrifuged, washed four times with ethanol and ultrapure water, and dried at 80 °C for 10 h in a vacuum drying oven. The product was obtained for subsequent studies. Illustration for the preparation is shown in Scheme S1. For comparison, CeO_2 NPs were also prepared using the similar method without adding PDI.

Characterization

High resolution transmission electron microscopy (HRTEM) images were obtained by a FEI Tecnai G2 F20 operated at 200 kV (https://www.fei.com). X-ray powder diffraction (XRD) was performed on a Rigaku D/Max-rB X-ray diffractometer with Cu Kα radiation (40 kV, 20 mA). Data was collected between $2\theta = 10$–80° with a step size of 0.02° (https://www.rigaku.com). Raman measurements were performed using a Raman spectrometer (Alpha 300 M+, WITEC) with the excitation light of 480 nm in the range of 100–2000 cm^{-1} (https://www.witec.de/). Fourier transform infrared (FT-IR) spectra were performed using a Thermo Nicolet 8700 spectrometer in the range of 4000–500 cm^{-1} (https://www.thermofisher.com). X-ray photoelectron spectroscopy (XPS) patterns were collected by a Thermo ESCALAB 250Xi Multifunctional imaging electron spectrometer with Al Kα radiation operated at 250 W (https://www.thermofisher.com). The electron spin resonance (ESR) spectra were obtained using a Bruker E580 with a

microwave bridge (receiver gain, 1×10^5; modulation amplitude, 2 G; microwave power, 10 mW; modulation frequency, 100 kHz) (https://www.bruker.com). UV-vis diffuse reflection spectra (DRS) were performed on a HITACHI UH4150 spectrophotometer in the range of 220~800 nm (https://www.hitachi-hightech.com).

Catalytic activity evaluation

The catalytic activity of NC sample was performed on the oxidation of TMB in the presence of H_2O_2 on a TU 1810 UV-vis spectrometer (Beijing General Analysis Instrument Co., Ltd. (http://www.pgeneral.com)). Briefly, 200 μL of 30 mg mL^{-1} NC suspension, 200 μL of 240 mM H_2O_2 and 200 μL of 1 mM TMB were carefully injected into 1400 μL buffer solution (pH 4.0), and reacted for 3 min. The ox-TMB is a blue product which has the maximum absorption at 652 nm. The buffers are acetate buffer (pH 2.0–5.0), phosphate buffer (pH 6.0–8.0) and Tris-HCl buffer (pH 9.0–10), respectively. The highest activity was defined as the 100% relative activity.

The GSH detection limit was determined through absorbance difference (ΔA) responses of NC + H_2O_2 + TMB system towards GSH. Illustration of GSH detection is shown in Scheme S2. After color reaction, GSH with different concentrations from 0 to 500 μM was added, and reacted for another 3 min, then immediately measured the absorbance at 652 nm. As for the determination of real GSH sample, the GSH tablet was firstly dissolved into ultrapure water to make a standard solution, and then diluted to different concentrations. The accuracy of this method can be measured by the recovery and relative standard deviation (RSD) between the determined concentration and the standard concentration.

Results and discussion

Catalyst characterization

From Fig. 1a, it can be seen that the irregular CeO_2 NPs with 10~20 nm in size are easy to agglomerate. Interestingly, NC (Fig. 1b) is found to be the uniform nanoparticle structure with the size of 3~5 nm, indicating that the introduction of PDI molecule plays an important role in the dispersion and morphology of CeO_2. As presented in Fig. 1c and d, the crystalline lattice on the CeO_2 NPs and NC fringed at ca. 0.310 nm is assigned to the (111) plane of fluorite-type CeO_2 [24, 25], which is

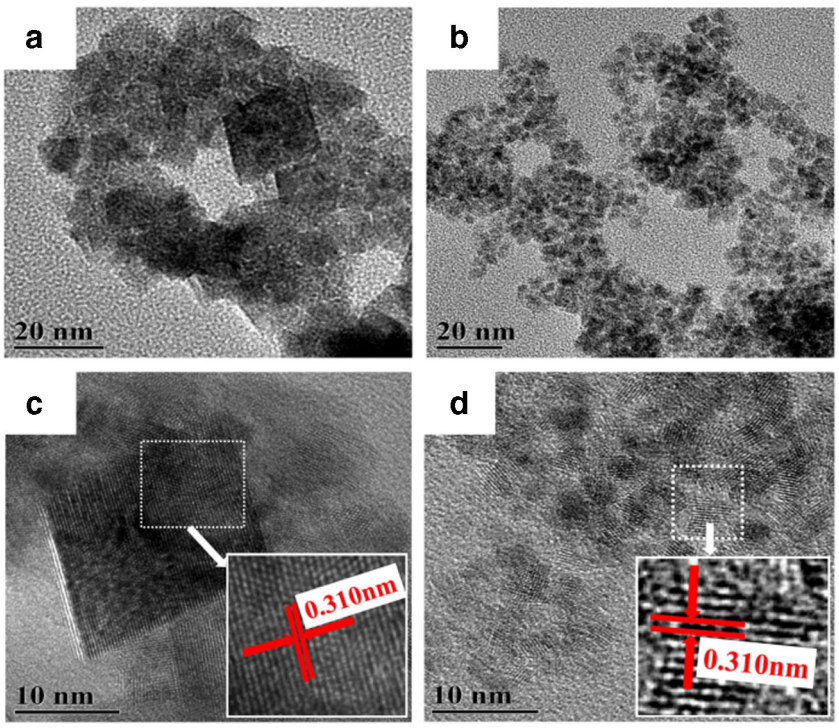

Fig. 1 HRTEM images of (**a**), (**c**) CeO_2 NPs and (**b**), (**d**) NC

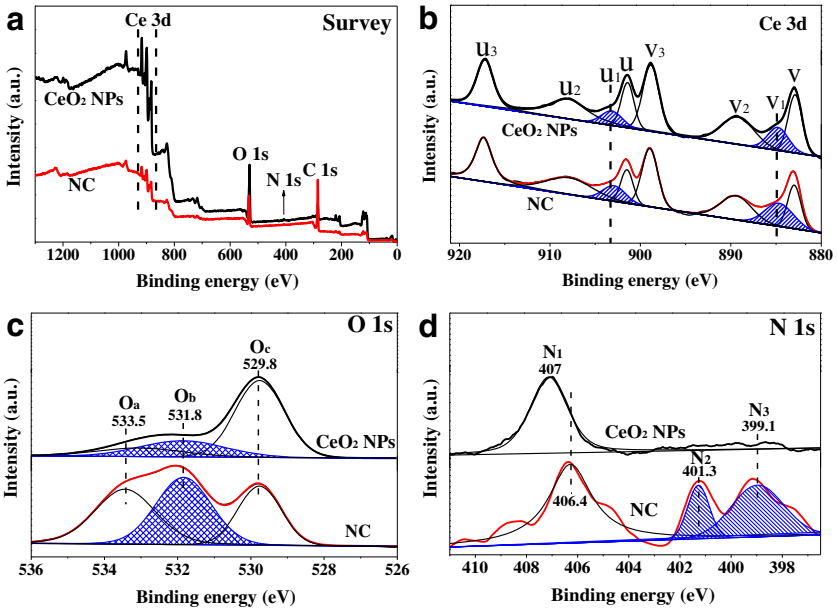

Fig. 2 XPS spectra of CeO_2 NPs and NC: **a** survey spectra; **b** Ce 3d; **c** O 1 s; **d** N 1 s

consistent with the XRD results (Fig. S1). In addition, the particle size of NC is obviously reduced which inevitably led to a large increase in specific surface area, and further provides more active species. Moreover, the distribution of Ce element is consistent with that of C and N (Fig. S2), suggesting the uniform distribution of PDI molecules on the CeO_2 NPs.

The valence states and surface atomic compositions of the samples were obtained by XPS. The survey spectra in Fig. 2a display that both CeO_2 NPs and NC contain Ce, N, O and C. In the Ce 3d spectra (Fig. 2b), the peaks marked as v, v_2, v_3, u, u_2 and u_3 correspond to Ce^{4+} species, while the peaks denoted by v_1 (884.9 eV) and u_1 (903.3 eV) are ascribed to Ce^{3+} with oxygen vacancies [26, 27]. The relative content of Ce^{3+} can be calculated by the ratio of Ce^{3+} peak area to that of the total Ce^{3+} and Ce^{4+} peak area, and the results are listed in Table S1 [28]. The relative concentration of Ce^{3+} on the surface of NC is 18.5%, obviously higher than that of CeO_2 NPs (13.1%). The formation of more Ce^{3+} ions associated with the oxygen vacancies is responsible for the enhanced activity [16]. Therefore, the loading of PDI increases the relative content of Ce^{3+}, thus resulting in the formation of more oxygen vacancies [29].

In the O 1 s spectra (Fig. 2c), adsorbed oxygen species (O_a) at 533.5 eV are attributed to hydroxyl water and/or carbonates, surface oxygen (O_b) at 531.8 eV is assigned to oxide defects, and lattice oxygen (O_c) at 529.8 eV [27, 29]. As can be seen in Table S1, more O_b is formed on the NC due to the efficient attachment between PDI molecules and CeO_2 NPs, indicating the existence of more surface active oxygen [30]. In the N 1 s spectra (Fig. 2d), for CeO_2 NPs, only one peak at 407 eV corresponds to the NO_3^- that adsorbed on CeO_2 NPs. However, for NC, the peaks at 401.3 and 399.1 eV can be assigned to the -N-CO- and -N-C- group [31, 32], verifying the presence of PDI molecules. The Raman and FT-IR results can also prove this conclusion (Fig. S3).

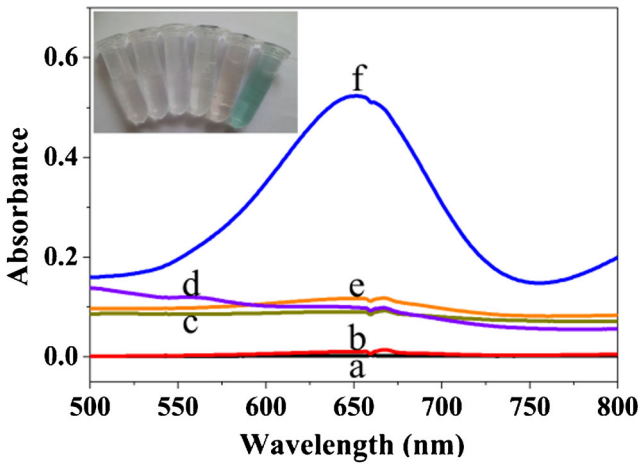

Fig. 3 UV-vis absorption spectra of different systems: **a**. TMB; **b**. TMB + H_2O_2; **c**. CeO_2 + TMB; **d**. CeO_2 + TMB + H_2O_2; **e**. NC + TMB; **f**. NC + TMB + H_2O_2. Conditions: pH = 4, RT, CeO_2 and NC 30 μg mL^{-1}, H_2O_2 24 mM, TMB 0.1 mM. The inset represents the colorimetric photographs (3 min)

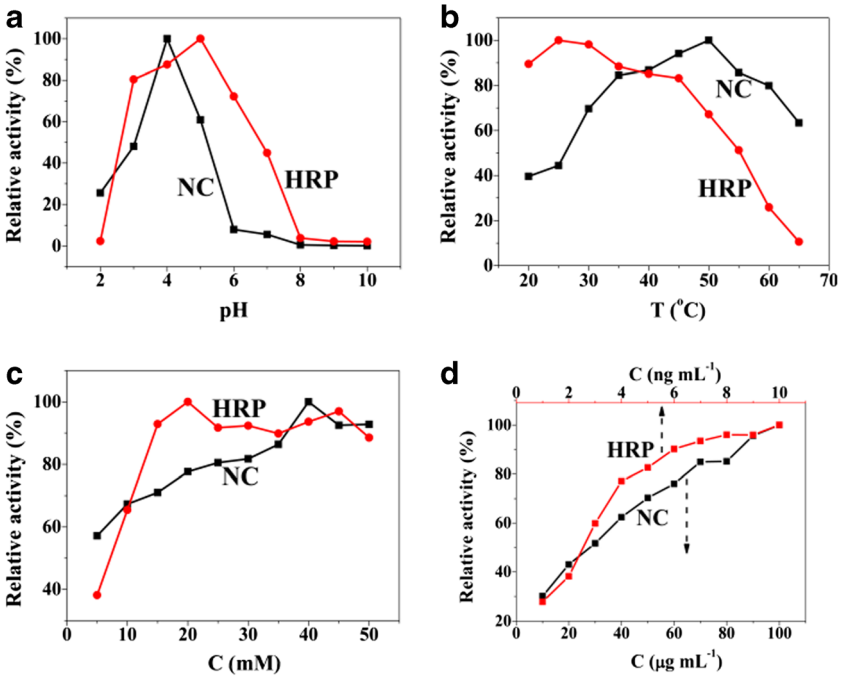

Fig. 4 Effect of (**a**) pH, **b** temperature, **c** H_2O_2 concentration and (**d**) catalyst concentration on the catalytic activity of HRP and NC. The data was collected at 652 nm

Catalytic activity

To primarily evaluate the peroxidase-like activity of NC, six different systems were reacted under the same conditions (Fig. 3). Inset is the corresponding photograph after reacting for 3 min. No obvious color change can be seen in the absence (a, c) and presence (b, d) of H_2O_2 before adding NC. And the TMB can also not be oxidized by NC without H_2O_2,

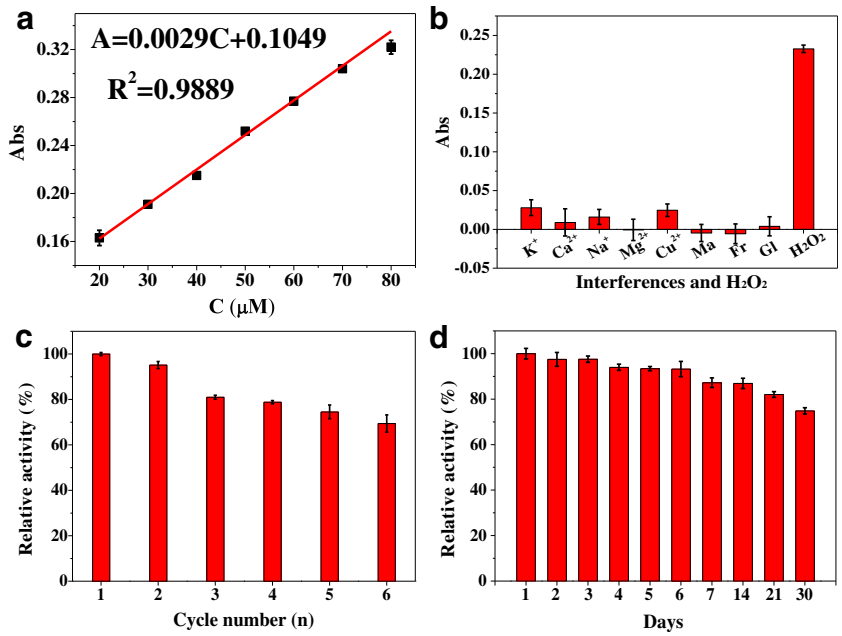

Fig. 5 **a** The H_2O_2 detection limit tests: H_2O_2 concentration varied from 10 to 100 μM; **b** Selectivity of NC towards H_2O_2 (1 mM) and interferents (5 mM); **c** Reusability and (**d**) durability performance of NC. The data was collected at 652 nm

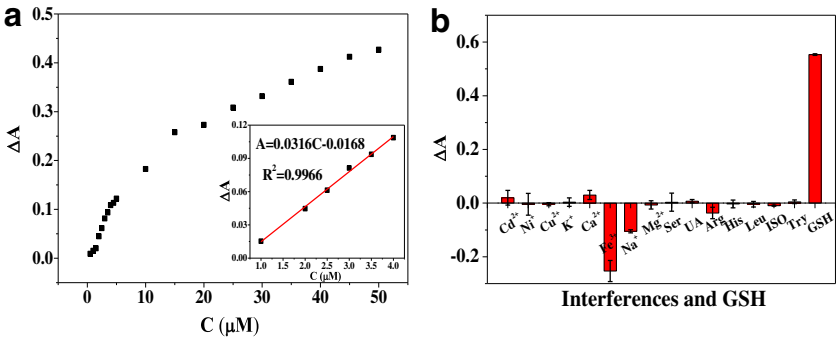

Fig. 6 **a** ΔA responses of NC + H_2O_2 + TMB system at 652 nm toward different GSH concentration from 0.5 to 50 μm, inset is the linear fitting curve from 1 to 4 μM; **b** Selectivity of NC towards interferences (500 μM) and GSH (50 μM)

indicating the catalyst has no oxidase-like activity (e). However, the blue color can be quickly observed once NC is added into the H_2O_2/TMB system, verifying that the NC possesses excellent peroxidase-like activity (f).

The comparative studies were conducted to understand the effect of pH, temperature, H_2O_2 concentration and catalyst concentration on the activity of HRP and NC. In Fig. 4a, the activity of NC reaches the maximum at pH 4.0 and decreases significantly at more acidic and/or alkaline pH, similar to some other mimics [14, 16]. However, the HRP shows high activity in a wider pH range from 3~6, and achieves the best effect at pH 5. Importantly, the NC exhibits high activity at higher temperature from 35 to 60 °C, while only when the temperature below 45 °C can HRP achieve the same effect (Fig. 4b). As shown in Fig. 4c and d, the influence of H_2O_2 concentration and catalyst concentration on the activity of HRP and NC are similar. The results indicate that NC can replace HRP to be catalyst for H_2O_2 determination. Although HRP is more effective in a wider pH range, the NC can be used in a higher temperature environment.

The LOD of H_2O_2 was determined by varying the H_2O_2 concentration from 10 to 100 μM and the TMB concentration was kept 100 μM. As shown in Fig. 5a, a linear response to H_2O_2 ranges from 20 to 80 μM with a LOD of 2.59 μM. The selectivity is evaluated using various metal ions, maltose, fructose and glucose all at concentration of 5 mM in place of 1 mM H_2O_2 under the same conditions. From Fig. 5b, it is obvious that the absorbance of these interferences can be negligible, suggesting the method is highly selective for H_2O_2. Besides, steady state kinetic tests prove that NC has a higher affinity towards TMB substrate in comparison with some reported mimic enzymes (Fig. S4 and Table S2) [33]. The reusability and durability of NC were also evaluated (Fig. 5c). After cycling used for six times, the NC still remains 70% of its initial activity. Considering the mass loss during centrifugal processes, the reusability of this NC catalyst is good. Although stored in a shady and dark place for a month, the activity of NC still keeps 75% (Fig. 5d). The excellent reusability and durability performance of NC are crucial to its industrial applications.

Table 1 Determination of glutathione (GSH) in the real injection sample

Standard (μM)	Found (μM)	Recovery (%)	RSD (%)
1	1.02	101.9	1.91
2	1.98	99.1	3.39
3	3.10	103.4	2.26
4	4.06	101.4	3.35
5	5.05	101.1	1.92

Based on the excellent activity of NC, a colorimetric method for detecting reduced glutathione (GSH) is constructed. From Fig. 6a, the absorbance difference (ΔA) exhibits a good linear relationship with the concentration of GSH ranging from 1 to 4 μM with a LOD of 0.92 μM. As shown in Fig. 6b, among various metal ions, only Fe^{3+} strongly promotes the catalytic activity of CeO_2, which has been proved by previous reports [13, 34]. For these amino acids, only GSH can severely reduce the reaction system. However, for colorimetric method based on peroxidase mimics, it is still a challenge to distinguish GSH from the materials with similar redox properties such as ascorbic acid and L-cysteine. When the system to be tested is confirmed has no these substances, this method exhibits good sensitivity and selectivity toward GSH determination.

The practical application for detecting real GSH sample was conducted under the optimal conditions based on the above colorimetric method. Every concentration was performed for three times under the same conditions and the results are shown in Table 1. The recoveries of GSH with five different concentrations are in the range from 99.1% to 102.4% and the relative standard deviation (RSD) values

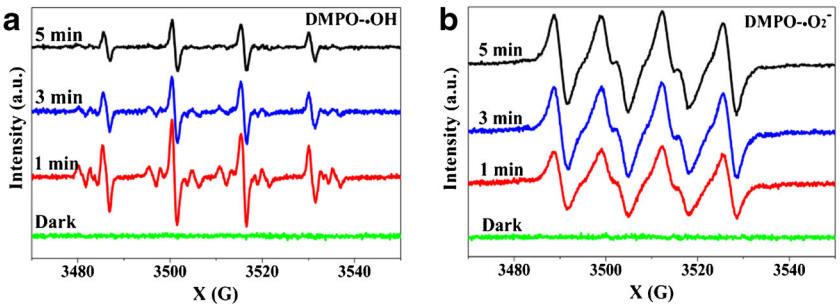

Fig. 7 DMPO spin-trapping ESR spectra for NC in (**a**) aqueous dispersion for DMPO-•OH and (**b**) methanol dispersion for DMPO-•O_2^-

are below 5%, indicating the potential in real sample analysis.

Possible mechanism

The ESR technique was employed to confirm active radicals using 5, 5-dimethyl-1-pyrroline N-oxide (DMPO) as the spin trapper [34, 35]. As shown in Fig. 7a and b, for NC, both DMSO-•OH and DMSO-•O_2^- signals can be clearly observed in the presence of light. However, no signals can be observed for both of them in dark. The results suggest that both •OH and •O_2^- radicals are the main active species during the catalytic process of NC in the presence of H_2O_2. Importantly, the catalytic reaction is triggered by light. Therefore, the band structures of PDI and CeO_2 were also studied by DRS technique (Fig. S5).

On the basis of these results, a possible mechanism for the catalytic oxidation of TMB/H_2O_2 system over NC catalyst is described in Scheme 1. On one hand, the conduction band (CB) of CeO_2 NPs is higher than that of PDI, so the electrons can be transferred easily from CeO_2 to PDI, and forming an electric field which facilitates the separation of electrons. Then the enriched electrons can be captured by dissolved O_2 in solution to form •O_2^-. On the other hand, the holes on the value band (VB) of CeO_2 which show strong oxide capability, are injected into the VB of PDI to oxidize H_2O_2, producing •OH radicals. The sufficient surface defects (Ce^{3+} ions and O-vacancies) on the surface of nano-CeO_2 are also active sites for catalytic reaction. At last, the colorless TMB is oxidized by •OH, •O_2^- and surface defects on the surfaces of CeO_2 NPs to form blue ox-TMB.

Conclusions

In conclusion, PDI functionalized CeO_2 nanocomposite (NC) can be prepared by a one-pot hydrothermal method and tested for peroxidase-like activity. After decorated by PDI, the surface of CeO_2 NPs presents more Ce^{3+} ions and active oxygen species. The composite catalyst exhibits superior activity at weakly acidic pH (4) and a broad temperature range (35~60 °C) in comparison with HRP. The colorimetric

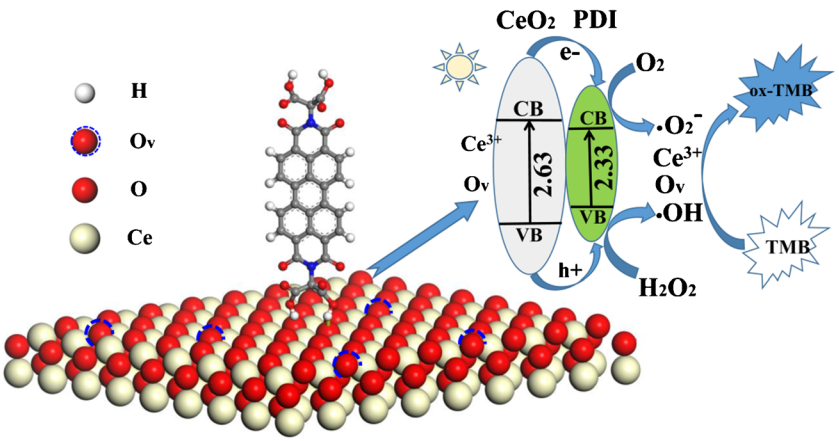

Scheme 1 Schematic diagram of electron-hole pair separation and the possible mechanism of NC.

determination of H_2O_2 shows a linear range from 20 to 80 μM with a LOD of 2.59 μM. And the NC presents excellent reusability and durability performance which are critical to its practical application. Besides, a colorimetric method for detecting GSH can be built which exhibits a linear relationship in the range from 1 to 4 μM with a LOD of 0.92 μM. The improved catalytic activity of NC catalyst is probably due to the high sensitivity of PDI towards visible light, the abundant surface defects of nano-CeO_2, and the easy electron transfer between PDI and nano-CeO_2. Although NC has narrow pH range with high catalytic activity and relative high limit of detection, it exhibits high activity at higher temperatures and can be reused.

Acknowledgments This work was supported by the National Natural Science Foundation of China (Grant No. 21271119), Natural Science Foundation of Shandong Province (Grant No. ZR2018MB002 and ZR2018MEE003), the SDUST Research Fund (2014TDJH104 and SDKDYC180366), and QUSTHX201904.

Compliance with ethical standards The author(s) declare that they have no competing interests.

References

1. Hu L, Liao H, Feng L, Wang M, Fu W (2018) Accelerating the peroxidase-like activity of gold nanoclusters at neutral pH for colorimetric detection of heparin and heparinase activity. Anal Chem 90 (10):6247–6252. https://doi.org/10.1021/acs.analchem.8b00885
2. Choleva TG, Gatselou VA, Tsogas GZ, Giokas DL (2017) Intrinsic peroxidase-like activity of rhodium nanoparticles, and their application to the colorimetric determination of hydrogen peroxide and glucose. Mikrochim Acta 185(1):22. https://doi.org/10.1007/s00604-017-2582-8
3. Sun Y, Wang R, Liu X, Shan G, Chen Y, Tong T, Liu Y (2018) Laser-induced formation of Au/Pt nanorods with peroxidase mimicking and SERS enhancement properties for application to the colorimetric determination of H_2O_2. Mikrochim Acta 185(9):445–454. https://doi.org/10.1007/s00604-018-2981-5
4. Chen S, Chi M, Zhu Y, Gao M, Wang C, Lu X (2018) A facile synthesis of superparamagnetic Fe_3O_4 nanofibers with superior peroxidase-like catalytic activity for sensitive colorimetric detection of L-cysteine. Appl Surf Sci 440:237–244. https://doi.org/10.1016/j.apsusc.2018.01.152
5. Hu AL, Liu YH, Deng HH, Hong GL, Liu AL, Lin XH, Xia XH, Chen W (2014) Fluorescent hydrogen peroxide sensor based on cupric oxide nanoparticles and its application for glucose and L-lactate detection. Biosens Bioelectron 61:374–378. https://doi.org/10.1016/j.bios.2014.05.048
6. Liu Q, Chen P, Xu Z, Chen M, Ding Y, Yue K, Xu J (2017) A facile strategy to prepare porphyrin functionalized ZnS nanoparticles and their peroxidase-like catalytic activity for colorimetric sensor of hydrogen peroxide and glucose. Sensor Actuat B-Chem 251:339–348. https://doi.org/10.1016/j.snb.2017.05.069
7. Shen JS, Wu JJ, Sun XY, Wu ZL, Gao P, Liu B (2017) Formaldehyde sensing based on the catalytic reaction of β-HgS nanocrystals. J Mater Chem C 5:3757–3764. https://doi.org/10.1039/C7TC00404D
8. Liu H, Wang B, Li D, Zeng X, Tang X, Gao Q, Cai J, Cai HH (2018) MoS_2 nanosheets with peroxidase mimicking activity as viable dual-mode optical probes for determination and imaging of intracellular hydrogen peroxide. Mikrochim Acta 185(6):287–295. https://doi.org/10.1007/s00604-018-2792-8
9. Gao P, Sun XY, Liu B, Lian HT, Liu XQ, Shen JS (2018) Cu MOF-based catalytic sensing for formaldehyde. J Mater Chem C 6(30): 8105–8114. https://doi.org/10.1039/c8tc01703d
10. Tan B, Wu WH, Liu X, Zhang YB, Quan X (2017) Fe_3O_4-AuNPs anchored 2D metal-organic framework nanosheets with DNA regulated switchable peroxidase-like activity. Nanoscale 9(47):18699–18710. https://doi.org/10.1039/c7nr05541b
11. Wang C, Tang G, Tan H (2018) Colorimetric determination of mercury(II) via the inhibition by ssDNA of the oxidase-like activity of a mixed valence state cerium-based metal-organic framework. Mikrochim Acta 185(10):475–482. https://doi.org/10.1007/s00604-018-3011-3
12. Lin X, Li S, He H, Wu Z, Wu J, Chen L, Ye D, Fu M (2018) Evolution of oxygen vacancies in MnO_x-CeO_2 mixed oxides for soot oxidation. Appl Catal B-Environ 223:91–102. https://doi.org/10.1016/j.apcatb.2017.06.071
13. Jampaiah D, Reddy T, Kandjani AE, Selvakannan PR, Sabri YM, Coyle VE, Shukla R, Bhargava SK (2016) Fe doped CeO_2 nanorods for enhanced peroxidase-like activity and their application towards glucose detection. J Mater Chem B 4(22):3874–3885. https://doi.org/10.1039/c6tb00422a
14. Huang F, Wang J, Chen W, Wan Y, Wang X, Cai N, Liu J, Yu F (2018) Synergistic peroxidase-like activity of CeO_2-coated hollow Fe_3O_4 nanocomposites as an enzymatic mimic for low detection limit of glucose. J Taiwan Inst Chem Eng 83:40–49. https://doi.org/10.1016/j.jtice.2017.12.011
15. Bracamonte MV, Melchionna M, Giuliani A, Nasi L, Tavagnacco C, Prato M, Fornasiero P (2017) H_2O_2 sensing enhancement by mutual integration of single walled carbon nanohorns with metal oxide catalysts: the CeO_2 case. Sensor Actuat B-Chem 239:923–932. https://doi.org/10.1016/j.snb.2016.08.112
16. Jampaiah D, Reddy TS, Coyle VE, Nafady A, Bhargava SK (2016) Co_3O_4@CeO_2 hybrid flower-like microspheres-a strong synergistic peroxidase-mimicking artificial enzyme with high sensitivity for glucose detection. J Mater Chem B 5(4):720–730. https://doi.org/10.1039/c6tb02750d
17. Song S, Wang X, Zhang H (2015) CeO_2-encapsulated noble metal nanocatalysts: enhanced activity and stability for catalytic application. NPG Asia Mater 7(5):e179–e179. https://doi.org/10.1038/am.2015.27
18. Wang J, Shi W, Liu D, Zhang Z, Zhu Y, Wang D (2017) Supramolecular organic nanofibers with highly efficient and stable visible light photooxidation performance. Appl Catals B-Environ 202:289–297. https://doi.org/10.1016/j.apcatb.2016.09.037
19. Zhang X, Lu Z, Ye L, Zhan C, Hou J, Zhang S, Jiang B, Zhao Y, Huang J, Zhang S, Liu Y, Shi Q, Liu Y, Yao J (2013) A potential perylene diimide dimer-based acceptor material for highly efficient solution-processed non-fullerene organic solar cells with 4.03% efficiency. Adv Mater 25(40):5791–5797. https://doi.org/10.1002/adma.201300897
20. Lv X, Yu M, Yang Y, Liu J, Liang D, Tang S, Liu D, Jin R (2018) Design of acceptors with high mobility via substitutions on dimeric perylene diimide for organic solar cells: a theoretical study. J Taiwan Inst Chem Eng 83:82–89. https://doi.org/10.1016/j.jtice.2017.11.025
21. Wang H, Zhao L, Liu X, Xu J, Hou W, Wang J, He E, Zhang R, Zhang H (2017) Novel hydrogen bonding composite based on copper phthalocyanine/perylene diimide derivatives p-n heterojunction with improved photocatalytic activity. Dyes Pigments 137:322–328. https://doi.org/10.1016/j.dyepig.2016.11.014
22. Büyükekşi SI, Karatay A, Acar N, Küçüköz B, Elmali A, Şengül A (2018) Syntheses and studies of electron/energy transfer of new dyads based on an unsymmetrical perylene diimide incorporating

chelating 1,10-phenanthroline and its corresponding squareplanar complexes with dichloroplatinu (II) and dichloropalladium (II). Dalton Trans 47(22):7422–7430. https://doi.org/10.1039/C8DT01135D

23. Shi Y, Wu H, Xue L, Li X (2012) Synthesis and properties of perylenetetracarboxylic diimide dimers linked at the bay position with conjugated chain of different length. J Colloid Interface Sci 365(1):172–177. https://doi.org/10.1016/j.jcis.2011.09.036
24. Yao W, Liu Y, Wu Z (2018) The promoting effect of CeO_2@Ce-O-P multi-core@shell structure on SO_2 tolerance for selective catalytic reduction of NO with NH_3 at low temperature. Appl Surf Sci 442:156–163. https://doi.org/10.1016/j.apsusc.2018.02.066
25. Lian J, Liu P, Li X, Bian B, Zhang X, Liu Z, Zhang X, Fan G, Gao L, Liu Q (2019) Multi-layer CeO_2-wrapped Ag_2S microspheres with enhanced peroxidase-like activity for sensitive detection of dopamine. Colloid Surface A 565:1–7. https://doi.org/10.1016/j.colsurfa.2018.12.047
26. Molinari M, Parker SC, Sayle DC, Islam MS (2012) Water adsorption and its effect on the stability of low index stoichiometric and reduced surfaces of ceria. J Phys Chem C 116(12):7073–7082. https://doi.org/10.1021/jp300576b
27. Pang J, Li W, Cao Z, Xu J, Li X, Zhang X (2018) Mesoporous Cu_2O-CeO_2 composite nanospheres with enhanced catalytic activity for 4-nitrophenol reduction. Appl Surf Sci 439:420–429. https://doi.org/10.1016/j.apsusc.2018.01.055
28. Wang Y, Shen X, Chen F (2014) Improving the catalytic activity of CeO_2/H_2O_2 system by sulfation pretreatment of CeO_2. J Mole Catal A-Chem 381:38–45. https://doi.org/10.1016/j.molcata.2013.10.003
29. Fan J, Wu X, Wu X, Liang Q, Ran R, Weng D (2008) Thermal ageing of Pt on low-surface-area CeO_2-ZrO_2-La_2O_3 mixed oxides: effect on the OSC performance. Appl Catal B-Environ 81(1–2):38–48. https://doi.org/10.1016/j.apcatb.2007.11.022
30. Mullins DR, Albrecht PM, Chen TL, Calaza FC, Biegalski MD, Christen HM, Overbury SH (2012) Water dissociation on CeO_2(100) and CeO_2(111) thin films. J Phys Chem C 116(36):19419–19428. https://doi.org/10.1021/jp306444h
31. Yamamoto K, Taneichi D (2000) A self-doped oligoaniline with two stable redox couples in a wide pH range. Macromol Chem Phys 201(1):6–11. https://doi.org/10.1002/(SICI)1521-3935(20000101)201:1<6::AID-MACP6>3.0.CO;2-3
32. Gao LF, Ju L, Cui H (2017) Chemiluminescent and fluorescent dual-signal graphene quantum dots and their application in pesticide sensing arrays. J Mater Chem C 5(31):7753–7758. https://doi.org/10.1039/C7TC01658A
33. Wang N, Duan J, Shi W, Zhai X, Guan F, Yang L, Hou B (2018) A 3-dimensional C/CeO_2 hollow nanostructure framework as a peroxidase mimetic, and its application to the colorimetric determination of hydrogen peroxide. Mikrochim Acta 185(9):417–424. https://doi.org/10.1007/s00604-018-2957-5
34. Wang W, Zhu Q, Qin F, Dai Q, Wang X (2018) Fe doped CeO_2 nanosheets as Fenton-like heterogeneous catalysts for degradation of salicylic acid. Chem Eng J 333:226–239. https://doi.org/10.1016/j.cej.2017.08.065
35. Zhang K, Wang J, Jiang W, Yao W, Yang H, Zhu Y (2018) Self-assembled perylene diimide based supramolecular heterojunction with Bi_2WO_6 for efficient visible-light-driven photocatalysis. Appl Catal B-Environ 232:175–181. https://doi.org/10.1016/j.apcatb.2018.03.059